Estuarine, Coastal and Shelf Science xxx (xxxx) 109858

Contents lists available at ScienceDirect

Estuarine, Coastal and Shelf Science

journal homepage: www.elsevier.com/locate/ecss

Variations in size and composition of dissolved organic matter in porewater and creek water during tidal cycles in a saltmarsh

Jingyu Wang [a], Zhaohui Zhang [a,*], Hui Lin [b]

[a] Institute of Marine Chemistry and Environment, Ocean College, Zhejiang University, 1 Zheda Road, Zhoushan, 316021, China
[b] Polar Research Institute of China, 1000 Xuelong Road, Shanghai, China

ARTICLE INFO

Keywords:
Saltmarsh
Dissolved organic matter
Fluorescence EEM
Flow field-flow fractionation
Porewater
Tidal pumping

ABSTRACT

Saltmarshes are biogeochemical hotspots for organic matter transformations, with exchange of dissolved organic matter (DOM) across the sediment-water interface. However, molecular size, a crucial property characterizing DOM, remains underexplored in the transformation processes of DOM constituents across this zone. Variations in DOM properties between porewater and creek water during tidal cycles were investigated during summer and autumn in a macrotidal saltmarsh, Hangzhou Bay, China, using flow field-flow fractionation (FlFFF) combined with fluorescence excitation-emission matrix and parallel factor analysis (EEM-PARAFAC). DOM from Andong saltmarsh exhibited a predominantly autochthonous origin, with protein-like compounds accounting for approximately 75% of the total fluorescent DOM. Dissolved organic carbon (DOC) concentration, aromaticity and humification of DOM in creek water negatively correlated with tidal levels. Principal component analysis revealed distinct differences in properties and composition of DOM between creek water and porewater. DOC concentration, fluorescence indices, and humic-like components in porewater fell between those of creek water during the flood and ebb tides. Moreover, humic-like components were primarily present in <10 kDa size-fraction, with a higher proportion (56.8%) in the medium-sized (2-20 kDa) fraction of creek water during autumn. Protein-like components were observed across <3 kDa, ~50 kDa and >100 kDa size ranges in both porewater and ebbing water. Seasonal river runoff and pulses of organic carbon incorporated into surface sediments likely influence the origins and molecular weight distribution of DOM in the saltmarsh. This study emphasized the compositional and molecular size dynamics of DOM over tidal cycles at the tidal marsh-estuarine margins of a river-dominated estuary.

1. Introduction

Dissolved organic matter (DOM) is the most mobile and actively cycling organic matter fraction, and influences a spectrum of biogeochemical processes of carbon dynamics, nutrient uptake, etc. in estuarine environments (Bolan et al., 2011). DOM in coastal waters, an important component in the global carbon cycle (Hedges, 1992), consist of a mix of allochthonous terrestrial inputs from wetlands and river runoffs, and autochthonous materials from primary production and other biological activities (Fellman et al., 2010; Stedmon and Nelson, 2015). Flocculation, photochemical and microbial degradation (Amon and Benner, 1996; Fasching et al., 2014) can modify not only the amount, but also the quality (i.e., chemical composition and molecular structure, etc.) of DOM during the transportation process (Chen and Jaffé, 2014). The dynamics of DOM in intertidal wetlands are complex, influenced by its diverse origins, rapid transformation, and hydrological processes, including tidal exchange and mixing of groundwater with surface water. A knowledge of variations in optical properties and composition of DOM throughout tidal cycles across this critical transition zone would be critical to better understand the interaction between riverine and marine DOM inputs, and biogeochemical transformation from organic matter mineralization.

The molecular size or weight distribution of DOM in aquatic environments is another dimension for characterizing DOM. Each DOM size class may have distinct source, chemical and molecular composition, reactivity, and biogeochemical functions (Guo et al., 1995; Skoog and Benner, 1997). Large size organic matters were more bioavailable and rapidly remineralized by microbes than smaller size classes (Benner and Amon, 2015). DOM with low molecular weight (LMW, <2.5 kDa) is often considered as the background pool of refractory materials in the water columns in the Pacific and Atlantic (Broek et al., 2020). The com-

* Corresponding author.
E-mail address: zhaohui_zhang@zju.edu.cn (Z. Zhang).

https://doi.org/10.1016/j.ecss.2026.109858
Received 10 December 2025; Received in revised form 26 March 2026; Accepted 26 March 2026

plexity and age of marine DOM increase with decreasing molecular size (Benner and Amon, 2015). Flow field-flow fractionation (FlFFF) is capable of simultaneous size separation and characterization (Alasonati et al., 2010; Stolpe et al., 2013), and has been used to track the mixing behavior of DOM in the estuarine environments (Xu et al., 2018; Lin et al., 2023), as well as along transects from rivers to coastal waters (Zhou et al., 2016). In most estuaries, molecular sizes decrease from land to sea (Gao et al., 2019; Zhao et al., 2024), probably due to microbial degradation and photo-bleaching during the transport processes. FlFFF coupling with fluorescence excitation-emission matrix measurements and parallel factor analysis (EEM-PARAFAC) can be used to characterize the size-distribution and fluorescent components of DOM within individual water sample (Lin and Guo, 2020).

Saltmarsh wetlands, characterized by high primary productivity and efficient carbon sequestration (Nellemann et al., 2009), are not only important blue carbon ecosystem, but also significant sources of DOM to estuaries. Up to 40% of DOM on the southeastern coastal shelf of the U.S. was estimated to come from saltmarshes (Moran and Hodson, 1994), while roughly 35% of total organic carbon (TOC) input to the U.S. East Coast estuaries was contributed by tidal wetlands (Herrmann et al., 2015). The export of DOM to the adjacent estuary in Taskinas marsh creek, Virginia, USA, was predominated by highly humic and aromatic chromophoric dissolved organic matter (CDOM) (Knobloch et al., 2022). On the other hand, the marsh-estuarine interface is subject to fluctuating biogeochemical processes through changing tides and seasons (Odum, 2002). Clark et al. (2008) showed production and output of protein- and humic-like materials at ebb tide in a river outlet and adjacent saltmarshes in California, USA. In contrast, protein-like components in two coastal marshes along the Yangtze River Estuary (YRE) presented no clear pattern on neither tidal nor seasonal scales (Zhang et al., 2022). Furthermore, effects of seasonality on DOM dynamics are most pronounced in sediments <100 cm depth of the upper tidal flat which is most influenced by tidal flushing (Seidel et al., 2014). Tidal pumping, the primary driver of porewater exchange, connects wetland sediments to coastal carbon reservoirs (Diggle et al., 2019; Guimond and Tamborski, 2021; Santos et al., 2021). However, the dynamic changes in composition and molecular weight of DOM between porewater and creek water in response to tidal variations remain unclear, hindering us from understanding the exchange of DOM between sediment and overlying water in saltmarshes.

Andong saltmarsh is located on the southwest bank of the funnel-shaped Hangzhou Bay, the largest macrotidal estuarine bay and one of the most developed areas in China (Zhou et al., 2019) (Fig. 1a). Compared with the northern half, the southern channel receives little sewage from the densely populated northern areas, making it a better representation of freshwater and marine water mixing (Zhou et al., 2019). Andong Shoal is an alluvial coast, formed by the accumulation of sediments from the Yangtze and Qiantang River (Wu et al., 2008). The porewater exchange rate was estimated about 5.60 ± 2.78 cm d^{-1} and the outwelling fluxes of dissolved inorganic carbon (DIC) was 3.2 times that of carbon burial (Zhu et al., 2022).

We investigated the dynamic variations of DOM in sediment porewater and creek water during tidal cycles in Andong saltmarsh. Riverine discharges in this region are substantially higher in summer due to heavy precipitation, a typical feature of monsoon climate. Considering that the composition and molecular weight of riverine CDOM tend to differ from those of marine CDOM (Zhou et al., 2016; Zhao et al., 2024), we conducted field samplings in October 2023 (autumn) and June 2024 (summer) to assess the effects of seasonal fluctuations in riverine discharge. Creek water and sediment porewater were collected *in situ* over two consecutive tidal cycles on the intertidal unvegetated mudflat, which is subject to strong flood and ebb currents. FlFFF coupled with EEM-PARAFAC analysis were applied to elucidate changes in fluorescence EEM spectra with molecular weight distribution within individual water sample. Selected creek water and sediment porewater at different tidal levels were analyzed for $d^{13}C$ of dissolved organic carbon (DOC) to help identify the origins of DOC. Our main objectives were to 1) characterize the optical properties and composition of DOM in saltmarsh water in response to tidal cycles; 2) elucidate the differences in properties of DOM between creek water and sediment porewater; 3) reveal variations in composition of fluorescent dissolved organic matter (FDOM) along molecular weight distribution within individual water sample; and 4) explore the influence of river runoff on the origins and composition of DOM. This study will provide more detailed data for future research about impacts on DOM in coastal ecosystems in response to climate and environmental change.

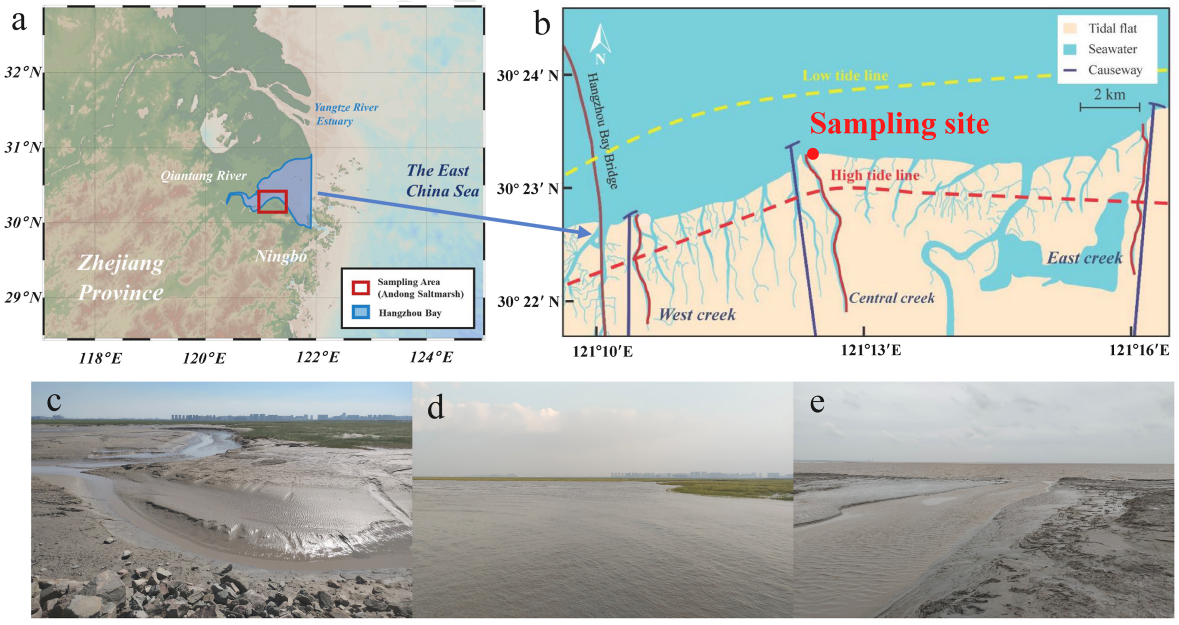

Fig. 1. Maps showing the location of Andong saltmarsh and sampling site. (a) A simplified map showing the location of Andong saltmarsh in China; (b) a map showing the research area in Andong saltmarsh, with tidal creeks and causeways marked; (c) a picture showing the mudflat at the end of the central creek at low tide; (d) a picture showing flooded saltmarsh at high tide; (e) a picture showing the central creek entering Hangzhou Bay at ebb tide.

2. Materials and methods

2.1. Study area

Andong saltmarsh is located on the south bank of Hangzhou Bay, China (30°14′N to 30°20′N, 121°05′E to 121°22′E) (Fig. 1a). It is in the subtropical monsoon regime with a mean annual temperature of 17.1 °C and mean annual rainfall of 1381 mm. The residue flow and sediments from the Yangtze River enter through the north and leaves through the south side of Hangzhou Bay (Xie et al., 2013) (Fig. 1a). Meanwhile, runoff from the Qiantang River also delivers a large amount of sediment, resulting in an increase of the saltmarsh area by 1.07 km^2 $year^{-1}$, rapid sedimentation rate of 2~4.5 cm $year^{-1}$, and seaward expansion of the mudflat at ~200 m a^{-1} (Huang et al., 2020). The monthly river discharge of the Qiantang River (near the Jiashao Bridge) and Yangtze River (Datong Station) are available from river discharge and related historical data from the Global Flood Awareness System (https://cds.climate.copernicus.eu/) and Yangtze River Water Resources Commission (http://www.cjw.gov.cn/zwzc/zjgb/), respectively.

Andong saltmarsh is predominated by irregular semidiurnal tides with a large tidal range averaged at 5.5 m (Fig. 1a and b), and strong rectilinear tidal currents. Saltmarsh coverage is about 3 km long and developed in the middle and upper parts of the intertidal zone, mainly composed of *Phragmites communis* and *Scirpus mariqueter*, while invasive *Spartina alterniflora* is intercalated with the native species. The intertidal zone has a developed creek system, and mudflat constitutes the major component of the low intertidal zone.

2.2. Collection of creek water and porewater during tidal cycles

Field works were conducted on 21 to 22 October, 2023 and 3 to 4 June 2024, at the entrance of the central tidal creek (30°23′53″ N, 121°12′22″ E), the largest and longest creek among the saltmarsh (Fig. 1b), which is presumably representative of the dynamic shifts between flood and ebb tides. Surface creek water samples were collected at an hourly interval during tidal cycles (Fig. 1c–e) by filling a 2 L polyethylene bottles using an overflow method (Chen and Hur, 2015). In total, 25 samples were collected in autumn 2023, and 26 samples in summer 2024 (Table S1). Creek waters were measured *in situ* for dissolved oxygen (DO), pH and salinity, using a portable YSI 556 MPS multi-parameter digital water quality meter.

Porewater were collected at 50 cm depth in the sediments *in situ* (Knoke et al., 2024) at hourly interval during the tidal cycle on 3 to 4 June 2024, using a CS-1200 Soil Pore Water Sampler, and a total of 27 porewater samples were collected. Porewater collection in October 2023 failed, as seawater inadvertently entered the sampling device at high tide because of inadequate sealing. Two drops of saturated $HgCl_2$ solution were added to collected water samples, which can eliminate the influence from the microorganism process. All water samples were filtered through precombusted (450 °C for 8 h) GF/F filters (Whatman, 0.7 μm) in the laboratory.

2.3. Measurements of DOC and δ^{13}C-DOC

DOC was measured using a TOC analyzer (Multi N/C 3100 TOC/TN, Analytik-Jena, Germany) with a non-dispersive infrared detector, at Nanjing Center, China Geological Survey. Sixteen creek water and porewater samples, collected at different tidal levels, were selected for carbon isotopes analysis of DOC using an IsoPrime 100 stable isotope ratio mass spectrometer (Elementar, USA) at the Third Institute of Oceanography, Ministry of Natural Resources. δ^{13}C values of DOC were reported relative to V-PDB with a standard deviation of ±0.2‰.

2.4. Ultrafiltration

Selected filtered water samples were concentrated through ultrafiltration for FlFFF analysis, using a stirred cell ultrafiltration unit (UFSC20001, Millipore Corporation, USA), equipped with 1 kDa ultrafiltration membrane filter (Ultracel regenerated cellulose, 63.5 mm diameter, Merck, USA), with the real cut off >1.33 kDa (Xu and Guo, 2017; Lin and Guo, 2020). The membrane filter was rinsed with 0.05 M NaOH solution followed by ultrapure water, before ultrafiltration.

2.5. Separation of DOM using FlFFF

The FlFFF system (AF4000, Postnova) was equipped with a 1 kDa membrane (polyether sulfone) under the separation channel. A carrier solution for optimal separation was prepared with 10 mM NaCl solution and 5 mM H_3BO_3 solution, and the pH was adjusted to 8.0 with NaOH solution (Lin and Guo, 2020). The retention time of DOM was calibrated using standard organic compounds with known molecular weights under identical conditions (Table S2; Figs. S1 and S2).

Flow settings were chosen based on previous studies (Lin and Guo, 2020; Zhou et al., 2016; Stolpe et al., 2014). Briefly, the focus, tip, and cross flow were initially set at 2.8, 0.2, 2.5 mL min^{-1}, respectively. After 5 min of focusing, the cross flow stayed at 2.5 mL min^{-1}, but outlet flow was set at 0.5 mL min^{-1}, the tip flow increased to 3.0 mL min^{-1}, and the focus flow gradually declined to zero, i.e. the FlFFF status shifted from focusing to eluting. After a 10-min elution, the flow field produced by cross flow gradually decreased to zero in 5 min, and the tip flow linearly declined from 3.0 to 0.5 mL min^{-1}.

Size-fractionated subsamples during elution were collected using precombusted glass vials at half-minute interval for offline fluorescence EEM measurements (Lin and Guo, 2020). An online UV absorbance detector (SPD-20A, Shimadzu) and two online fluorescence detectors (RF-20A, Shimadzu) were applied to measure CDOM, humic-like fluorophores (peak C, E_x/E_m = 350/450 nm) and tryptophan/protein-like fluorophores (peak T, E_x/E_m = 275/340 nm) changes, respectively, across its colloidal size continuum (Figs. S3–S5).

2.6. UV-visible absorption spectra

Absorption spectra of CDOM in creek water and porewater over the wavelength range from 250 to 750 nm were measured on a SPECORD 50 Plus UV-VIS spectrophotometer (Jena, Germany), using a 10 mm quartz cuvette, and ultrapure water as a blank. CDOM absorption coefficients at 254 nm (a_{254}) were calculated using the equation: a_{254} (m^{-1}) = $2.303 \times A(254\,nm)/l$, where a_{254} is the Naperian absorption coefficient at 254 nm, A(254 nm) is the absorbance at 254 nm, and l is the path length of the cuvette (in meters) (Lin and Guo, 2020). $SUVA_{254}$, an indicator of aromaticity, was calculated as: $SUVA_{254} = A(254\,nm)/(DOC \times l)$, with a dimension of L/m/mg-C (Weishaar et al., 2003). Spectral slopes between 275 and 295 nm ($S_{275\text{-}295}$ in nm^{-1}) were calculated using the following equation: $\alpha_\lambda = \alpha_{\lambda_0} e^{-S_{275-295}(\lambda-\lambda_0)}$.

2.7. Measurement of fluorescence EEM spectra and PARAFAC analysis

EEM spectra of creek water and porewater, as well as the FlFFF-fractionated subsamples were measured on an Aqualog absorption-fluorescence spectrometer (Horiba, Japan). Excitation and emission spectra were acquired over the ranges of 250 to 450 nm and from 220 to 600 nm at 5 nm interval, respectively (Fig. S6). Ultrapure water or carrier solution was referenced to eliminate background noise. First and second orders of Raman and Rayleigh scattering peaks were eliminated.

PARAFAC analysis was performed on the MATLAB 2022b (MathWorks) using the drEEM toolbox, with the EEM dataset from both bulk water samples and FlFFF-fractionated subsamples. The PARAFAC models were constrained to non-negative values, and the results were vali-

dated using split-half analysis (Fig. S7) (Lin and Guo, 2020). Four fluorescent components were identified and uploaded to OpenFluor for comparison with existing components (Murphy et al., 2013). C1 could be considered a semi-labile terrestrial DOM component (Weigelhofer et al., 2020), C2 indicated high molecular weight (HMW) DOM with high aromaticity (Shutova et al., 2014; Pitta and Zeri, 2021), C3 demonstrated typical protein-like tyrosine features linked to microbial activities (Osburn et al., 2018; Yang et al., 2019), and C4 exhibited an autochthonous tryptophan-like fluorescence peak T (Catalá et al., 2015; Dall'Osto et al., 2022).

2.8. Statistical analysis

Based on the results of the Kolmogorov-Smirnov and Levene tests, an ANOVA or Kruskal-Wallis test was performed to analyze the differences in DOM properties between creek water and porewater. Pearson or Spearman correlation tests were applied to explore the relationships between optical properties and composition of DOM, tidal heights, and salinity, with a significance level of 0.05 adopted for all analyses. To further investigate factors affecting DOM characteristics in porewater and creek water during tidal cycles, principal component analysis (PCA) was conducted. All series of data were log-transformed to produce a PCA dataset that was unaffected by negative bias or closure (Yunker et al., 2005). A Kaiser-Meyer-Olkin (KMO) value of 0.695 and significant Bartlett's test result ($p < 0.001$) indicated that PCA could be applied to creek water dataset (Cai et al., 2019). Similarly, PCA was applicable to the overall water samples dataset (KMO = 0.744; Bartlett's test, $p < 0.001$). All analyses were carried out using SPSS 26.0 and Origin 2025b software.

3. Results

3.1. Dynamic changes in multiple parameters in creek water and porewater during tidal cycles

3.1.1. Hydrological feature and physicochemical parameters

In October 2023, the monthly river discharge of the Yangtze River and Qiantang River reached 7.3×10^{10} m^3 and 2.4×10^5 m^3, respectively, while in June 2024, they were recorded at 1.1×10^{11} m^3 and 1.1×10^7 m^3. The tidal heights in Andong saltmarsh ranged between 1.3 and 3.8 m in October 2023, and from 0.5 to 3.8 m in June 2024 (Fig. 2; Tables S3 and S4). Salinity in the creek water decreased from 6.7 at the ebb tide to 5.5 at the flood tide in June 2024 (Fig. 2; Table S3).

Nitrate concentration in creek water ranged from 32.9 to 92.7 μM, exhibiting a pattern consistent with tidal levels (Spearman's correlation test, r = 0.763, $p < 0.001$) (Fig. 2a–S8a; Table 1). They were significantly higher than those in the porewater (3.5~13.3 μM) (Fig. 2b; Welch ANOVA test, $p < 0.001$). DO concentrations in porewater (2-4.3 mg L^{-1}) were also significantly lower than those in creek water (5.1-8.4 mg L^{-1}) (Kruskal-Wallis test, $p < 0.001$), and increased with rising tide (Fig. 2a and b). pH levels in both creek water in October 2023 and porewater in June 2024 showed no correlation with tidal levels (Fig. 2b and c; Tables S3 and S5).

3.1.2. Concentration and $\delta^{13}C$ of DOC

In June, 2024, concentrations of DOC in creek water ranged from 1.6 to 4.2 mg-C/L (Fig. 2a; Table S3), forming a negative correlation with tide height (Spearman's correlation test, r = −0.789, $p < 0.001$) (Fig. S8b; Table 1). Concentrations of DOC in porewater (2.3 ± 0.1 mg-C/L) were intermediate between those in creek water during the flood (1.3-2.6 mg-C/L) and ebb (2.9-4.2 mg-C/L) tides (Fig. 2a and b; Tables S3 and S5). δ^{13}C-DOC values in creek water during the ebb tide ranged from −27.9‰ to −26.2‰, similar to those observed in sediment porewater (−27.5‰ to −26.4‰), exhibiting no significant correlation with tidal heights (Fig. 3a; Table S6). In October, 2023, δ^{13}C-DOC in creek water during the ebb tides (−28.0‰~ −27.6‰) were slightly more negative than those during the flood tides (−27.0‰~ −26.8‰) (Fig. 3b; Table S6).

3.1.3. Optical properties of DOM in creek water and porewater

In June 2024, a_{254} in creek water during the ebb tide (15.4-23.9 m^{-1}) were higher than those during the flood tides (8.7-12.7 m^{-1}) (Pearson's correlation test, r = −0.798, $p < 0.001$) (Fig. 2d–S8c; S3), whereas $SUVA_{254}$ in creek water showed the opposite pattern (2.5-3.5 and 2.2-2.8 L/mg-C/m for flood and ebb tide, respectively, Spearman's correlation test, r = −0.791, $p < 0.001$) (Fig. 2d–S8d, Table 1, S3). The values of a_{254} and $S_{275\text{-}295}$ in porewater were averaged at 10.6 ± 2.1 m^{-1} and 0.026 ± 0.003 nm^{-1}, respectively, significantly higher than those in creek water (Fig. 2d and e; Tables S3 and S5) (One way and Welch ANOVA test, $p < 0.001$). There was significant difference in $S_{275\text{-}295}$ in creek water between June 2024 and October 2023 (Fig. 2d and f; Tables S3 and S4) (One way ANOVA test, $p = 0.003$).

3.1.4. Fluorescence components and properties of DOM

Fluorescence EEM spectra of DOM in the creek water and porewater consisted predominantly of protein-like (peak T; E_x/E_m = 275/320 nm) and humic-like (peak A: E_x/E_m = 250/450 nm; peak C: E_x/E_m = 320-360/420-460 nm) substances (Fig. S6). The humification index (HIX)

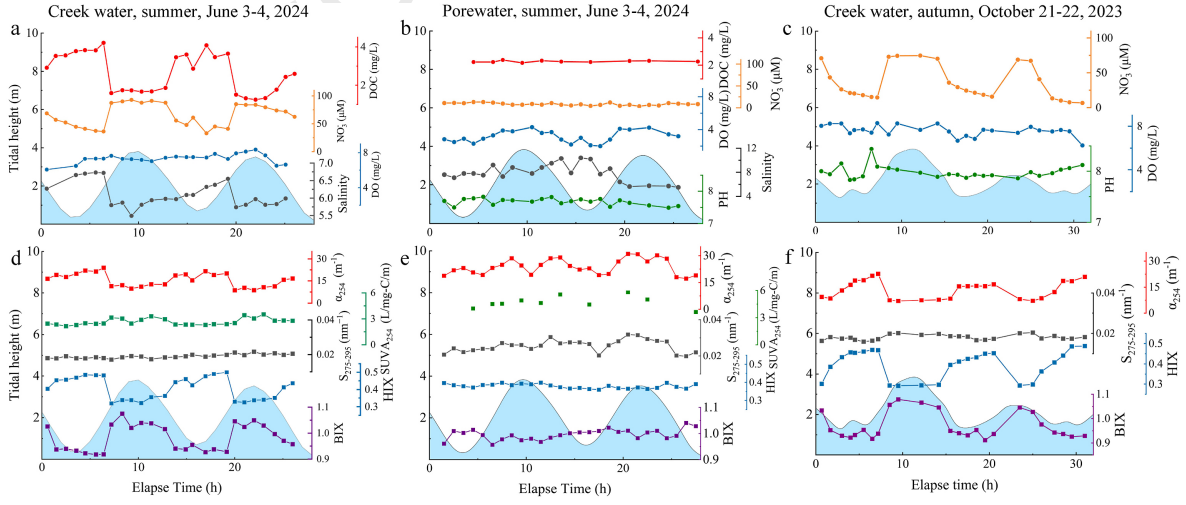

Fig. 2. Tidal variations of DOC concentration, optical properties, and fluorescence intensities of DOM in creek water (a, b) and porewater (c, d) during a tidal cycle in summer, and in creek water during autumn (e, f), in Andong saltmarsh.

Table 1
Correlation coefficients between tidal heights and various parameters in creek water and porewater collected from Andong saltmarsh.

	Creek water (summer)		Porewater (summer)		Creek water (autumn)	
NO3-	rs = 0.763	p < 0.001	r = −0.375	p = 0.054	rs = 0.561	p = 0.004
DOC	rs = −0.789		-			
a254	r = −0.798		r = 0.505	p = 0.007	rs = −0.341	p = 0.095
S275-295	r = 0.246	p = 0.226	r = 0.519	p = 0.006	r = 0.498	p = 0.011
SUVA254	rs = 0.791	p < 0.001	-			
HIX	rs = −0.746		rs = 0.093	p = 0.643	rs = −0.567	p = 0.003
BIX	rs = 0.737		r = −0.42	p = 0.029	rs = 0.651	p < 0.001
C1%	rs = −0.765		rs = 0.147	p = 0.465	rs = −0.635	p = 0.001
C2%	rs = −0.745		r = 0.163	p = 0.416	rs = −0.601	
C3%	rs = 0.763		rs = −0.301	p = 0.127	rs = 0.61	
C4%	rs = −0.773		rs = 0.434	p = 0.024	r = −0.513	p = 0.009

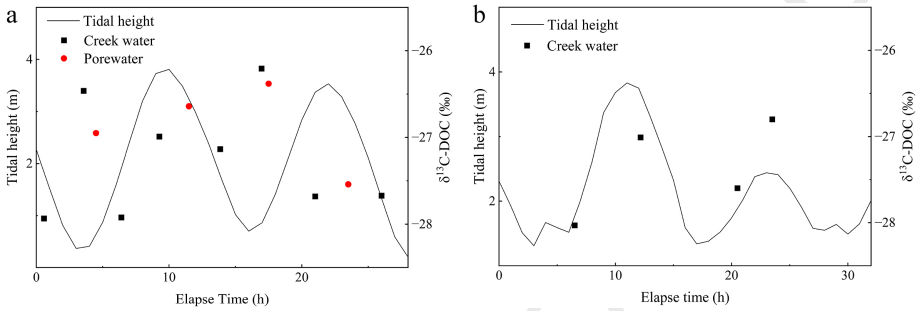

Fig. 3. $\delta^{13}C$ values of dissolved organic carbon (DOC) in water samples collected during different tidal phases in June 2024 (a) and October 2023 (b).

of CDOM in creek water in June 2024 decreased from 0.50 at the ebb tide to 0.32 at the flood tide (Spearman's correlation test, r = −0.746, $p < 0.001$), while the biological index (BIX) increased from 0.92 at ebb tide to 1.07 at flood tide (Spearman's correlation test, r = 0.737, $p < 0.001$) (Fig. 2d–S8f, S8g; Table 1, S3). HIX (0.38 ± 0.02) and BIX (1.00 ± 0.03) in porewater were intermediate between those in creek water during the flood and ebb tides (Fig. 2d and e; Tables S3 and S5).

Four fluorescence components were identified in both creek water and porewater, C1(E_x/E_m: <260 (320)/410), C2(E_x/E_m:<255 (375)/490), C3(E_x/E_m:280/317), C4(E_x/E_m: <250 (290)/344) (Fig. 4a). Humic-like components C1 and C2 in the ebbing water were significantly higher than those in the flood tides (Spearman's correlation test, r = −0.765 and −0.745, respectively, $p < 0.001$) (Fig. 4b and e, S8h, S8i), but those in porewater were intermediate between the levels in creek water during the flood and ebb tides (Fig. 4b and c). Protein-like components C3 and C4 in porewater were significantly higher than those in creek water (Kruskal Wallis test, $p < 0.001$). Furthermore, there were significant differences in C3 and C4 between creek water samples collected in June 2024 and October 2023 (Kruskal Wallis test, $p < 0.001$ and $p = 0.001$ for C3 and C4, respectively), but there were no significant differences in C1 and C2 (Fig. 4b and d). Additionally, the (C3 + C4)/(C1 + C2) ratio and HIX in creek water from both June 2024 and October 2003 exhibited inverse correlations (Spearman's correlation test, r = −0.951and −0.752, respectively, $p < 0.001$) (Tables S3 and S4).

3.2. Differences in DOM molecular size between porewater and creek water

UV_{254} absorbance and fluorescence intensities in the creek water during the ebb tides were roughly higher than those during the flood tides in June 2024 (Fig. 5, S3-S5), partly due to higher DOC concentration. UV_{254} absorbance and humic-like fluorescence in porewater were intermediate between those in creek water during the ebb and flood tides, while protein-like fluorescent intensity was higher than both (Fig. 5, S3-S5). UV_{254} signals in both creek water and porewater samples exhibited an overlapping peak in the <10 kDa range (Fig. 5a, S5). $Fluor_{350/450}$ (humic-like) in water samples from June 2024 showed a shoulder peak, which were more pronounced in October 2023 (Fig. 5b–S5). $Fluor_{275/340}$ (protein-like) exhibited a single narrow peak in all water samples, while had a secondary peak around 50 kDa size region in porewater (Fig. 5c–S5).

DOM were further fractionated into five size fractions, <1 kDa, 1-2 kDa, 2-20 kDa, 20-200 kDa, and >200 kDa (Fig. S9). Creek water in autumn 2023 contained a higher proportion of medium-sized (2-20 kDa, 59.3%) and fewer small-sized (1-2 kDa, 15.3%) colloids compared to 51.7% and 17.8%, respectively, in summer 2024 (Fig. S9a). Similarly, humic-like ($Fluo_{350/450}$) of creek water in autumn 2023 displayed a higher percentage of medium-sized (2-20 kDa, 56.8%) and fewer small-sized colloids (1-2 kDa, 20.0%) compared to those in summer 2024 (43.0% and 21.9%, respectively) (Fig. S9b). In contrast, protein-like substances ($Fluo_{275/340}$) were predominantly partitioned into the <1 kDa fraction (24.1-28.4%), followed by the >200 kDa (20.4-27.7%) and 1-2 kDa (18.4-20.7%) size fractions (Fig. S9c). Moreover, the size distribution in porewater during summer 2024 was similar to those in creek water, with 2-20 kDa and 1-2 kDa fractions accounting for 52.2 and 19.4%, respectively, except higher proportion of DOM in the 20-200 kDa range (14.9%) (Fig. S9).

3.3. Molecular size-dependent EEM spectra and DOM properties

The application of FlFFF combined with offline EEM measurements showed the fluorescence EEM characteristics of DOM exhibited changes along the molecular size distribution across creek water and porewater (Figs. S10 and S11). Fluorophores characterized with peaks A (E_x/E_m = 260/400-460 nm) and C (E_x/E_m = 320-360/420-460 nm) were primarily observed in the 1.3-10.6 kDa fractions, and faded away gradually with increasing size (Figs. S10 and S11). Fluorophores associated with peak B (E_x/E_m = 275/305 nm) appeared mostly in the ~50 kDa and >100 kDa fractions in porewater and ebbing water, but less prevalent in creek water during the flood tides (Figs. S10 and S11).

Humic-like components C1 and C2 were predominantly found in the

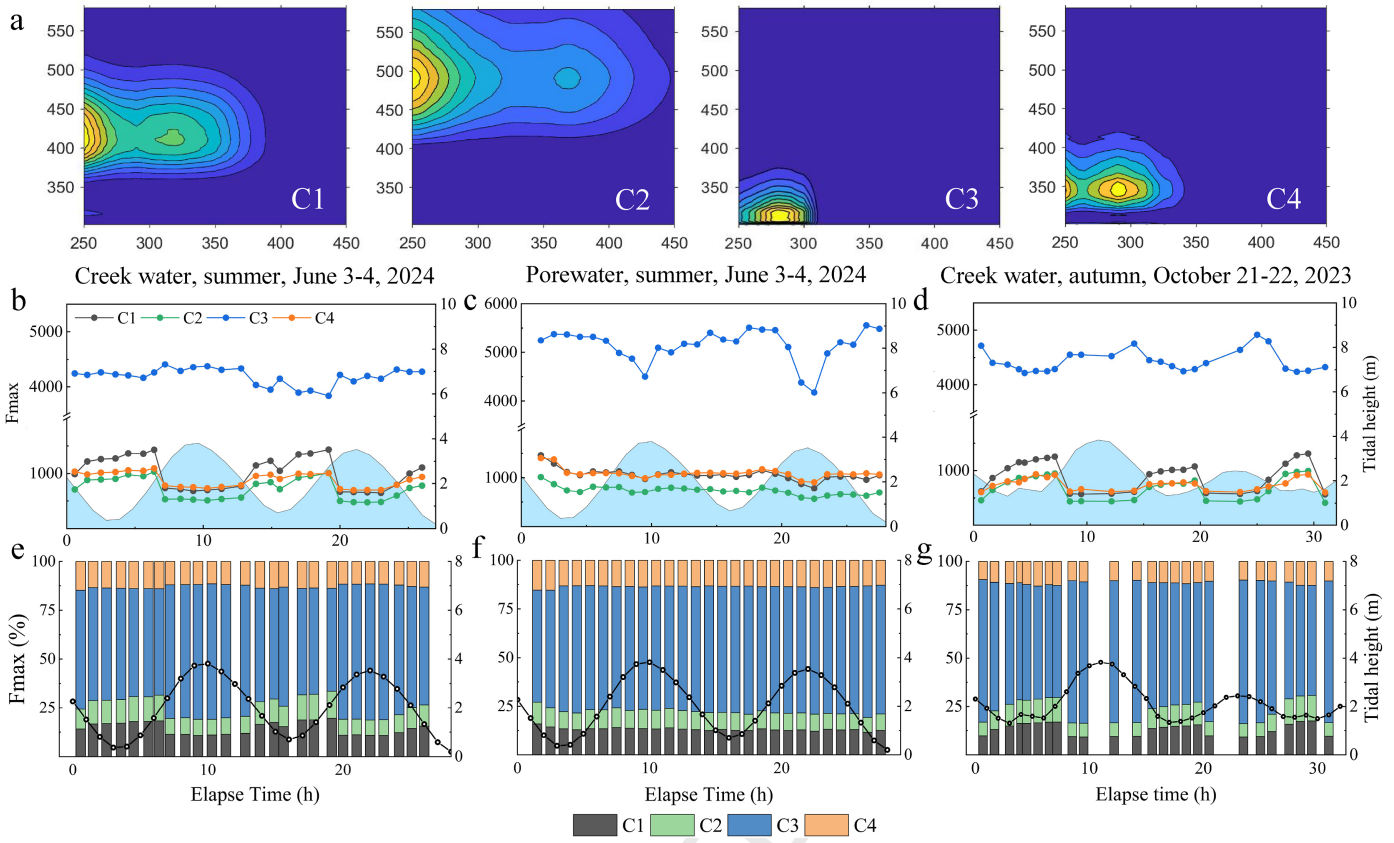

Fig. 4. Variations of PARAFAC components Fmax in response to tidal levels in Andong saltmarsh. (a) Four PARAFAC components derived from EEM data; the variations of PARAFAC components in creek water (b), porewater collected in June 2024 (c), and creek water collected in October 2023 (d) during the tidal cycle; (e-g) tidal variations of PARAFAC components Fmax (%) in Andong saltmarsh.

<20 kDa size range, while protein-like components C3 and C4 exhibited a distinct peak in the <10 kDa fraction, with additional peaks around 50 kDa and >100 kDa (Fig. S12a). Fluorescence indices also demonstrated dynamic changes across molecular sizes within each porewater and creek water sample. BIX initially decreased and then increased, whereas HIX varied in the opposite direction (Fig. S12b), indicating that highly humified components of DOM had a molecular weight of approximately 3 kDa.

4. Discussion

4.1. Impacts of river runoff and changing season on the origins of DOM

Salinity increased notably from the upstream to the downstream, especially pronounced in the southern half of Hangzhou Bay, reflecting a physical mixing of riverine freshwater and saltwater (Zhou et al., 2019). In October, 2023, monthly river discharge from the Qiantang River and Yangtze River decreased to 2.4×10^5 m^3 and 7.3×10^{10} m^3, respectively. The relatively small volume of freshwater in the tidal creek was significantly affected by salt tide intrusion (Li et al., 2019), although this influence was not as severe as in the Bay of Cádiz, Spain (a Mediterranean estuary), where riverine inputs are more limited or absent during the dry season, producing a negative hydrological budget and, consequently, hypersalinity and an inverse circulation pattern (Catalá et al., 2015). Previous study indicated that the salinity of dilute water in the YRE ranged from 15.8 to 27.4, and salinity at the mouth of Hangzhou Bay was recorded at 11.1 during autumn 2018 (Zhang et al., 2021).

$d^{13}C$ value of DOC in creek water during ebb tide (−28.0∼ −27.6‰) were slightly more negative than those during the flood tide (−27.0∼ −26.8‰) (Fig. 3; Table S6). The more negative values observed were likely derived from terrestrial sources, such as debris of marsh plants and soil leachates (Tzortziou et al., 2008), and DOM during flood tide was a mixture containing some marine-sourced phytoplankton-derived DOM. Furthermore, the protein-like material in creek water exhibited a slight increase during flood tide in autumn, which may be associated with the prevalence of the marine influence under low water discharges and anthropogenic pollution in estuary (Amaral et al., 2020).

In June 2024, the monthly discharge of the Qiantang River and the Yangtze River was relatively large, reaching 1.1×10^7 m^3 and 1.1×10^{11} m^3, respectively. There was a negative correlation between salinity in the creek water of the Andong saltmarsh and tidal heights (Spearman's correlation test r = −0.768, p = 0.001) (Fig. 6a; Table 1, S3), suggesting that tidal water in the creek partially came from the freshwater runoff of Qiantang River and Yangtze River. Although there was no significant correlation between $d^{13}C$-DOC in creek water (−27.9 to −26.2‰) and tidal height (Fig. 3; Table S6), $d^{13}C$-DOC during flood tide (−27.9∼ −27.0‰) were close to those in surface water of the YRE in July, 2017 (∼−28‰) (Wang et al., 2021). Changes in seasonal delivery of freshwater may influence composition of DOM (Martineac et al., 2021). A previous study indicated that along the gradient from the Mississippi River fresh water end-member station to an offshore station in the Gulf of Mexico, $\delta^{13}C$ values gradually increased from −26.2‰ to −21.8‰ with increasing salinity (Guo et al., 2009), and terrigenous DOM enrichment in the estuarine water, driven by increased runoff (Tzortziou et al., 2015; Amaral et al., 2020), results in a significant enhancement of the terrigenous signature of DOM throughout the estuary (Medeiros et al., 2015). River discharge was the primary driver of changes in the composition of DOM at the mouth of the Altamaha River, a marsh-dominated estuary (Letourneau et al., 2021) and in Jiulong River coastal estuary (Chen et al., 2021).

On the other hand, $d^{13}C$ of DOC in creek water during the ebb

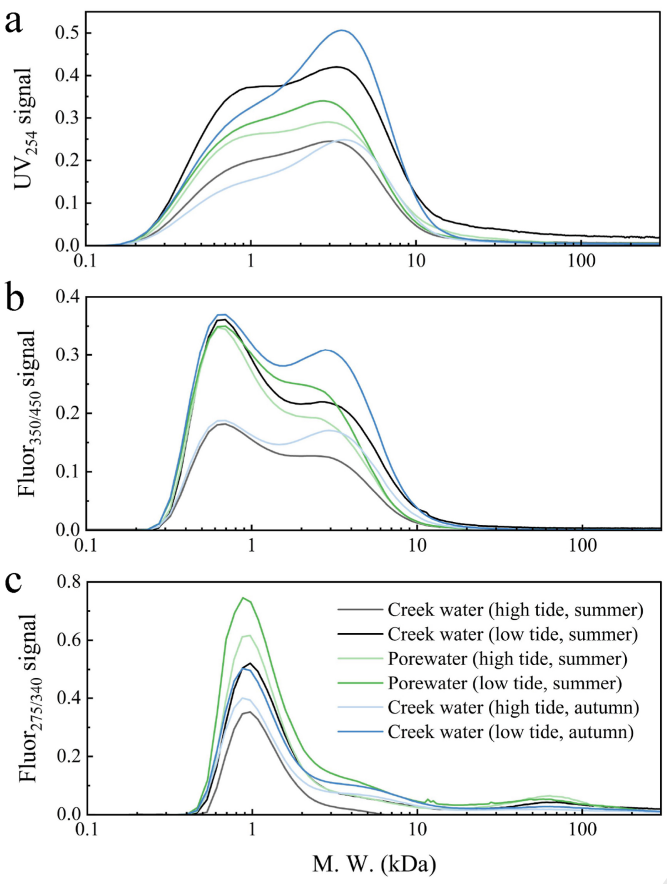

Fig. 5. FlFFF fractograms of DOM in creek water and porewater in Andong saltmarsh: UV absorbance at 254 nm (a), humic-like fluorescence at E_x/E_m = 350/450 nm (b), and protein-like fluorescence at E_x/E_m = 275/340 nm (c). A logarithmic scale was used for the x-axis, representing molecular weight.

tide (−27.1∼ −26.2‰) closely resemble those in sediment porewater (−27.5∼ −26.4‰) (Fig. 3; Table S6), which were more negative than the $d^{13}C$ value in porewater of top layers in East China Sea (ECS) (−26.0∼ −23.2‰) (Li et al., 2020), as the latter may have more marine sourced DOM. The average $d^{13}C$ values of sediments along two creeks in Andong saltmarsh were −23.8 ± 0.2‰ and −24.0 ± 0.2‰, indicating contributions from microbial biomass rich in protein and carbohydrates (Yuan et al., 2017), which can increase $d^{13}C$ values in soil organic materials (Ehleringer et al., 2000). The $\delta^{13}C$-DOC range in Andong saltmarsh is substantially narrower and more positive than that in the Sage Lot Pond Salt Marsh, MA, USA (−29.0 ± 3.7‰), which has been attributed to selective mineralization, the production of $\delta^{13}C$-depleted bacterial biomass, and methane-derived DOC (Eagle et al., 2025), and is also narrower than that in the Altamaha River Estuary in Georgia, southeastern U.S., associated with saltwater marsh vegetation (−25.5∼ −19‰) (Otero et al., 2003).

4.2. Influence of tidal cycles on DOM dynamics

PCA of the optical properties and composition of DOM in creek water collected from Andong saltmarsh in June 2024 revealed that PC1 and PC2 accounted for 84.2% and 9.0%, respectively, of the variance in DOM (Fig. 7a). Both DOC and a_{254} show positive correlations with HIX, humic-like components (C1, C2), and negative correlations with NO_3^- and BIX. Flood tide samples grouped with negative PC1 scores are associated with proteinaceous compounds exhibiting higher BIX. The loading values of PC1 showed a significantly positive relationship with humification- and aromaticity-related parameters, highlighting the dominant role of tidal hydrology, while PC2 seems to reflect the impact of biogeochemical reactions (Zhang et al., 2022). The tidal change in optical properties of DOM in creek water was consistent and qualitatively similar for both summer and autumn in the saltmarsh, except for the $S_{275\text{-}295}$ value. CDOM quality (absorption spectral slopes, fluorescence component ratios) was also less variable seasonally in the brackish marshes of Chesapeake Bay, a trend influenced by the gradual release of DOM from tidal marsh soils, which buffered DOM export from temperate marshes (Logozzo et al., 2021).

The correlation between tidal heights and DOM properties was less significant than anticipated (Table 1; Fig. S8). A potential disparate effect on DOM properties was observed across tidal cycles, deviating from the expected sinusoidal temporal pattern (Liu et al., 2025). The water flow from the adjacent estuary into the marsh, across the sampling site, and inundate the intertidal zone was swift, while the ebb tide retreated more gradually. When the tidal level rises, concentration of DOC, value of a_{254}, HIX, and humic-like components C1, C2 in creek water synchronous declined sharply from their highest values within an hour (Figs. 2 and 3). Labile organic matter formed from planktonic primary production in estuaries (Osburn et al., 2015), leading to higher BIX value and NO_3^- concentration in creek water. With continuous infiltration of surface water into sediment pores, protein-like component C3 in porewater showed a notable decrease, likely attributed to dilution of surface water (Fig. 4c). Meantime, DO in porewater decreased from 4.3 to 2.0 mg L^{-1} due to consumption for mineralization of organic matter (Amaral et al., 2021).

During the ebb tide, DOC, a_{254}, HIX, and C1, C2 in creek water gradually increased and reached simultaneously their maxima indicating the outflow of aromatic and humic substances into overlying water, while NO_3^- and BIX decreased. Most of relatively recalcitrant DOM, probably from anoxic sedimentary porewaters (Clark et al., 2014), is drained from the marsh during ebb tides when water stage is below bankfull depth (Nelson et al., 2017; Menendez et al., 2022). The negative correlations between concentration of DOC, aromaticity and humification of DOM in surface water and tide levels, were reported in Taskinas marsh creeks (Knobloch et al., 2022), in a saltmarsh-mangrove ecotone (Xiao et al., 2023), and in other coastal wetlands along the YRE (Zhang et al., 2022). Although no discernible pattern was observed in the variation of protein-like components C3 and C4 throughout the tidal cycles, likely due to their stronger association with biological processes (Fellman et al., 2010), a higher proportion of humic-like material (29.8 ± 2.2%) was observed during low tide, while protein-like substances (79.6 ± 2.1%) predominated during high tide in June 2024. These trends were more pronounced in October 2023, with 27.8 ± 2.1% for humic-like material and 82.5 ± 2.2% for protein-like substances.

Salinity exhibited significant relationships with the properties of DOM in creek water (Fig. 6; Table S3). Significant positive correlations were found between salinity and the concentration of DOC, a_{254}, HIX, C1(%), C2(%), and C4(%) (Spearman's correlation test, r = 0.876, 0.908, 0.905, 0.875, 0.855, 0.835, respectively, $p < 0.001$). In contrast, significant negative correlations were observed between salinity and NO_3^- concentration, BIX, C3(%) (Spearman's correlation test, r = −0.85, −0.81, −0.851, respectively, $p < 0.001$) in creek water collected in June 2024.

4.3. Similarities and differences in DOM properties between creek water and porewater

No significant differences were observed in the fluorescence spectral shapes or fluorescent component types of DOM between creek water and porewater—characteristics that reflect the changes in the composition and chemical structure of DOM (Tzortziou et al., 2008)—suggesting that exchange occurs at the sediment-water interface. However, there were differences in the fluorescence and absorption, component concentrations, and molecular weight distribution of DOM between creek water and porewater. Porewater is physically isolated by sediments in which geochemical transformations differ from those occurring in tidal creeks, and its accumulation and dynamics of DOM are largely dependent on re-

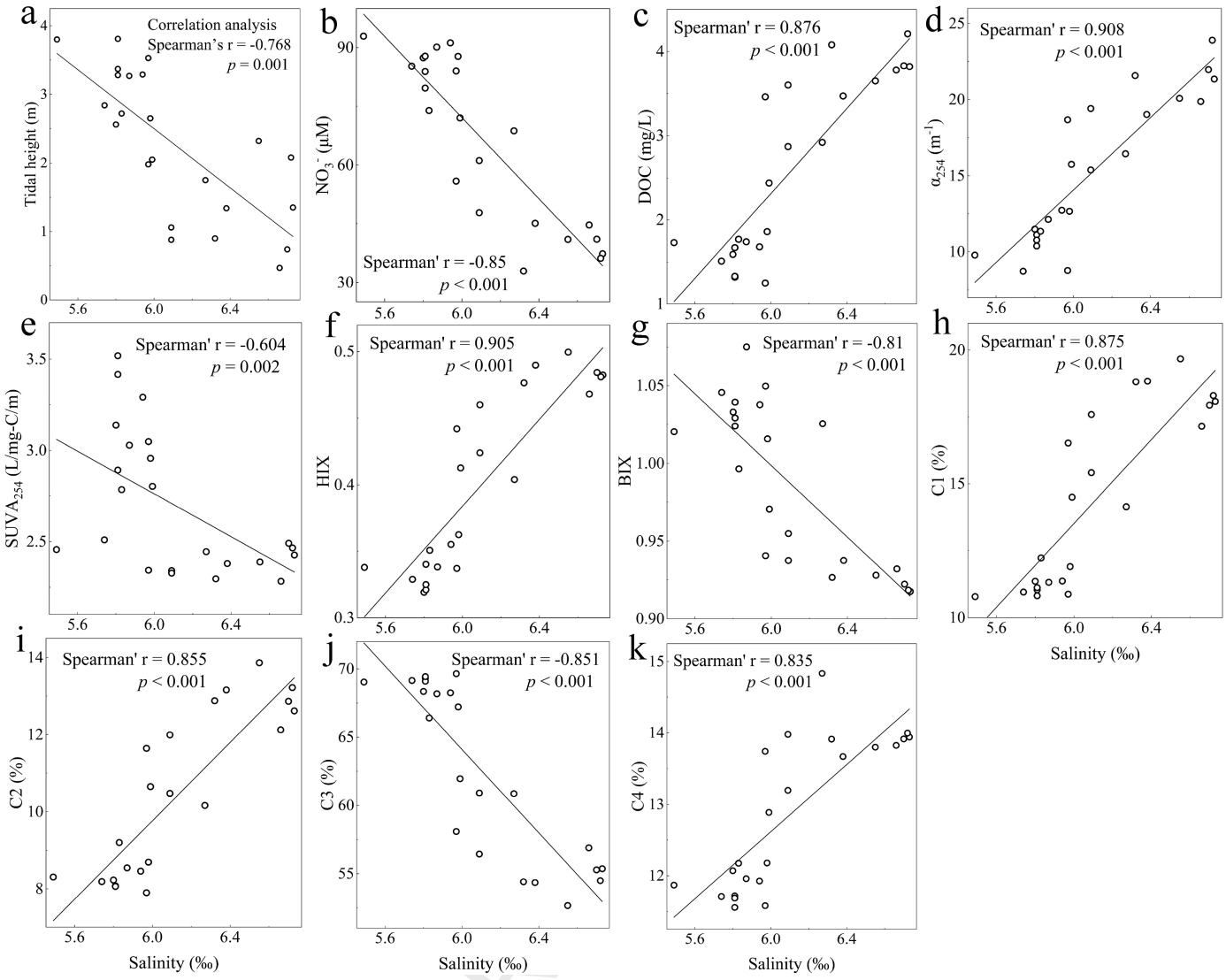

Fig. 6. Relationships between salinity and tidal level (a), concentration of NO_3^- (b), dissolved organic carbon (DOC) (c), a_{254} (d), $SUVA_{254}$ (e), HIX (f), BIX (g), and the PARAFAC-derived components C1-C4 (h-k) in the creek water collected from Andong saltmarsh in June 2024.

dox conditions (Nebbioso and Piccolo, 2013). The multivariate statistical analysis based on optical properties of DOM in all water samples collected across different tidal stages in summer and autumn demonstrated that porewater and creek water were clearly distinguished and exhibited unique DOM characteristics on the PC1 and PC2 axes (Fig. 7b). DOM signal of porewater was identified by higher humification (α_{254}), lower molecular weight ($S_{275\text{-}295}$) and an increased presence of protein-like materials compared to creek water (Figs. 2 and 3).

Concentration of DOC, value of BIX, HIX, and humic-like components (C1, C2) in porewater were intermediate between those in creek water during the flood and ebb tides (Figs. 2 and 3), but showed no significant variation with tidal changes. In contrast, porewater DOM (5 cm depth) in the Liaohe coastal wetland was characterized by lower protein-like fluorescence and BIX, but higher humification, humic-like fluorescent components and aromaticity index than surface water DOM (Lu et al., 2020). DOC pool in surface sediments (3 cm depth) of sandy area in the YRE and ECS was rather transient due to its high reactivity and mobility (Li et al., 2024). Such gaps may stem from differences in sampling method and depth. Nevertheless, both studies suggested that DOM in porewater exhibits a higher degree of humification and aromaticity than surface water (Lu et al., 2020; Schiebel et al., 2020). HIX remained relatively low in creek water (0.41 ± 0.06) and porewater (0.38 ± 0.02) in the Andong saltmarsh (Fig. 2), indicating the source of DOM with scarce humic materials, but high autotrophic productivity and significant marine influence (Huguet et al., 2009).

Protein-like components C3 and C4 in porewater were significantly higher than those in creek water (Fig. 4), and predominantly contributed to the CDOM fluorescence (77.7 ± 1.5%), suggesting enhanced microbial production in the sediment (Huguet et al., 2009). This finding aligns with reports that the enrichment of less degraded and HMW protein-like fluorescent components in sediment porewater of sandy area in the YRE and adjacent ECS shelf (Li et al., 2024; Zhou et al., 2022), as anoxic conditions and high microbial activities may help preserve protein-like compounds in porewater, as seen in the Black Sea and Rhône River delta (Schmidt et al., 2017). When porewater seeps into the creek and is exposed to oxic, light-rich conditions, protein-like compounds increase relative to aromatic ones, which are more susceptible to photodegradation or flocculation (Kaiser et al., 1996; Cory et al., 2015). However, the turbid water in creek of Andong saltmarsh shelter DOM from direct photodegradation, keeping humic-like material relatively enriched in the ebbing water. Moreover, eutrophication induced by nutrient inputs from the Yangtze River and the western coasts of the ECS was most pronounced in the near field plume (salinity <30) over the inner shelf (0-50 m) of the ECS (Malone and Newton, 2020; Xiao et al., 2021). This

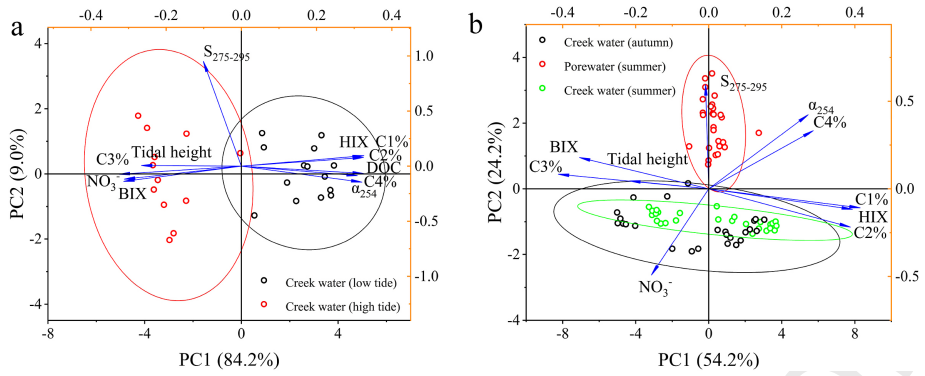

Fig. 7. Principal component analysis (PCA) of water samples from Andong saltmarsh. (a) Loadings and scores of the first two PCA components for DOM optical properties in creek water collected in June 2024. (b) Loadings and scores of the first two PCA components for DOM optical properties in all water samples.

may lead to the proliferation of bloom species (Xiao et al., 2021; Li et al., 2014; Lu et al., 2014), with DOM being predominantly autochthonous and containing a higher content of protein-like material in coastal water. Additionally, increases in algal blooms due to anthropogenic nutrient input also may increase the autochthonous production of DOM in Daliao river coastal wetlands (He et al., 2022).

4.4. Heterogeneity in molecular size changes of DOM in creek water and porewater

The continuous size distribution of DOM provided by FlFFF was consistent with the EEM spectra of size fractions and the PARAFAC analysis results for individual water samples (Fig. 5, S9-12). The proportion of medium-sized (2-20 kDa) DOM in creek water during autumn (59.3%) was higher than that in summer (51.7%), predominantly in the form of humic-like substances (56.8%) (Fig. 5, S10). One possible explanation for this difference is that marsh-derived DOM from plants typically exhibits a relatively high MW and is more aromatic and humic in composition relative to estuarine material (Menendez et al., 2022). Although the maximum soil sorption capacity increase with rising salinity, the binding affinity of DOC decrease (Pinsonneault et al., 2021). The pulses of organic carbon from marsh plants incorporated into surface sediments during autumn (Schiebel et al., 2018), together with the estuarine mixing driven by hydraulic forces, may have given rise to the abundance of humic-like materials with higher MW during both ebb and flood tides. Another explanation is destabilization of terrestrial colloidal humic substances during mixing with seawater (Sholkovitz, 1975), leading to an increase in their mean size through colloid aggregation (Batchelli et al., 2009). The extent of flocculation of organic carbon and humic substances is highly salinity-dependent (Sholkovitz, 1975), and increasing salinity may also marginally enhance sediment flocculation (Deng et al., 2023).

$Fluor_{275/340}$ in porewater exhibited a clear secondary peak around 50 kDa in the FlFFF-derived fractograms (Fig. 5). The fluorophore associated with peak B (protein-like components C3 and C4) was found in the size ranges of approximately 50 kDa and >100 kDa in both porewater and receding creek water, but were less prevalent in creek water during flood tide (Fig. 5, S9-12). Although variations in DOM were partly driven by changes in DOC amounts during tidal cycles, this phenomenon could also be ascribed to diminished presence of protein-like materials with higher MW in creek water during flood tide. There were higher MW components in the deeper porewaters compared to those in shallower porewater and surface water in the restored Brookhurst salt marsh, California, USA, as the latter experienced enhanced oxidative processing (photochemical or microbial breakdown) (Clark et al., 2019). Another explanation is that, despite the different extents in decline, both carbohydrates and protein-like substances underwent substantial microbial utilization during incubation and followed a similar transformation pathway, from the <1 kDa fraction to colloids (1 kDa-0.45 μm), and further to microparticles (>0.45 μm) (Xu et al., 2018). Additionally, certain protein-like FDOM showed high intensity in the deep regions of the Bay of Bengal and had bulk molecular weights (10-50 kDa and >50 kDa fractions), the formation of which appears to depend on elevated salinity, as microbes polymerize FDOM to form colloidal particles that protect it from extreme salinity and other environmental stresses (Niloy et al., 2023).

High protein-like to humic-like ratio or BIX/HIX ratio were observed in the <2 and >20 kDa size ranges (Fig. S12), suggesting that protein-like components are more abundant in either lower (<2 kDa) or higher (>20 kDa) molecular weight fractions, while humic-like components are more common in the 2-20 kDa range. Freshly produced DOM from autochthonous sources is usually larger in size than more degraded, humic-like DOM (Amon and Benner, 1996; Fellman et al., 2010; Williams et al., 2010). In addition, the relative abundance of protein-like C3 and C4 in porewater and creek water from the Andong saltmarsh showed a significant peak at <10 kDa, with greater enrichment of protein-like materials of smaller MW, particularly in porewater (Fig. S12). This distribution differs from DOM in Milwaukee River (Lin and Guo, 2020), where humic-like substances may be more abundant.

5. Conclusions

This study investigated variability in optical properties, composition, and molecular size distribution of DOM in both sediment porewater and creek water during tidal cycles in a macrotidal saltmarsh in China, which may enhance our understanding of the modulation of DOM at the tidal marsh-estuarine margins of a river-dominated estuary under climate change. Time-series water samples *in situ* were collected on the mudflat at hourly time interval. Concentration of DOC, aromaticity and humification of DOM and humic-like components in the ebbing water were higher than those during flood tides. Meanwhile, principal component analysis highlighted the distinct optical signatures between sediment porewater and creek water in the saltmarsh and revealed the dynamics of DOM in creek water in response to the tidal pumping. Protein-like component C3 in porewater decreased during the highest tide level. In addition, creek water in autumn contained a higher proportion of medium-sized (2-20 kDa) DOM, primarily composed of humic-like substances. These substances are likely derived from soil leachates and debris of marsh plants or from the enhanced flocculation of river-born humic-like materials due to increasing salinity. In contrast, protein-like materials were also present in the higher molecular size fractions (~50 kDa and >100 kDa), especially in porewater, likely due to reduced oxidation treatment (photochemical degradation) and high microbial activities. Seasonal river runoff and organic carbon pulses in surface sediments may influence the origins and molecular weight distribution of DOM in a saltmarsh. The limitations of this study include the lack of DOC fluxes and the absence of water samples collected in spring and winter. Further sampling efforts are required to account for additional influencing factors and more ac-

curately capture the seasonal variations in DOM. Meanwhile, advanced techniques such as ultrahigh-resolution mass spectrometry and Fourier transform ion cyclotron resonance mass spectrometry (FT-ICR MS) could be employed, which can help uncover the potential heterogeneity and dynamic variations of DOM at the molecular level.

CRediT authorship contribution statement

Jingyu Wang: Data curation, Formal analysis, Investigation, Methodology, Writing – original draft. **Zhaohui Zhang:** Conceptualization, Funding acquisition, Investigation, Methodology, Project administration, Resources, Supervision, Validation, Writing – review & editing. **Hui Lin:** Data curation, Methodology.

Declaration of competing interest

The authors declare that they have no known competing financial interests or personal relationships that could have appeared to influence the work reported in this paper.

Acknowledgments

This research was supported by Zhejiang Provincial Natural Science Foundation of China under Grant No. LZ23D060002 (Z.Z). We are grateful to Yifei Xu, Shaokang Chen, Yang Wang, Junjie Zhang and Mingli He for the assistance in field work. We are indebted to two anonymous reviewers for their insightful comments and critical criticisms, which greatly help improve our manuscript.

Appendix A. Supplementary data

Supplementary data to this article can be found online at https://doi.org/10.1016/j.ecss.2026.109858.

Data availability

Data will be made available on request.

References

Alasonati, E., Dubascoux, S., Lespes, G., Slaveykova, V.I., 2010. Assessment of metal-extracellular polymeric substances interactions by asymmetrical flow field-flow fractionation coupled to inductively coupled plasma mass spectrometry. Environ. Chem. 7, 215–223. https://doi.org/10.1071/EN09148.

Amaral, V., Romera-Castillo, C., Forja, J., 2021. Submarine mud volcanoes as a source of chromophoric dissolved organic matter to the deep waters of the Gulf of Cádiz. Sci. Rep. 11, 3200. https://doi.org/10.1038/s41598-021-82632-3.

Amaral, V., Romera-Castillo, C., García-Delgado, M., Gómez Parra, A., Forja, J., 2020. Distribution of dissolved organic matter in estuaries of the southern Iberian Atlantic Basin: sources, behavior and export to the coastal zone. Mar. Chem. 226, 103857. https://doi.org/10.1016/j.marchem.2020.103857.

Amon, R., Benner, R., 1996. Bacterial utilization of different size classes of dissolved organic matter. Limnol. Oceanogr. 41 (1), 41–51. https://doi.org/10.4319/lo.1996.41.1.0041.

Batchelli, S., Muller, F.L.L., Baalousha, M., Lead, J.R., 2009. Size fractionation and optical properties of colloids in an organic-rich estuary (Thurso, UK). Mar. Chem. 113, 227–237. https://doi.org/10.1016/j.marchem.2009.02.006.

Benner, R., Amon, M.W.R., 2015. The size-reactivity continuum of major bioelements in the ocean. Ann. Rev. Mar. Sci 7, 185–205. https://doi.org/10.1146/annurev-marine-010213-135126.

Bolan, N.S., Adriano, D.C., Kunhikrishnan, A., James, T., McDowell, R., Senesi, N., 2011. Chapter one - dissolved organic matter: Biogeochemistry, dynamics, and environmental significance in soils. Adv. Agron. 110, 1–75. https://doi.org/10.1016/B978-0-12-385531-2.00001-3.

Broek, T.A.B., Walker, B.D., Guilderson, T.P., Vaughn, J.S., Mason, H.E., McCarthy, M.D., 2020. Low molecular weight dissolved organic carbon: aging, compositional changes, and selective utilization during global ocean circulation. Glob. Biogeochem. Cycles 34 (6). https://doi.org/10.1029/2020GB006547. e2020GB006547.

Cai, L.M., Wang, Q.S., Wen, H.H., Luo, J., Wang, S., 2019. Heavy metals in agricultural soils from a typical township in Guangdong Province, China: occurrences and spatial distribution. Ecotoxicol. Environ. Saf. 168, 184–191. https://doi.org/10.1016/j.ecoenv.2018.10.092.

Catalá, T.S., Reche, I., Fuentes-Lema, A., Romera-Castillo, C., Nieto-Cid, M., Ortega-Retuerta, E., Calvo, E., Alvarez, M., Marrasé, C., Stedmon, C.A., Alvarez-Salgado, X.A., 2015. Turnover time of fluorescent dissolved organic matter in the dark global ocean. Nat. Commun. 6, 5986. https://doi.org/10.1038/ncomms6986.

Chen, Q., Chen, F., Gonsior, M., Li, Y., Wang, Y., He, C., Cai, R., Xu, J., Wang, Y., Xu, D., Sun, J., Zhang, T., Shi, Q., Jiao, N., Zheng, Q., 2021. Correspondence between DOM molecules and microbial community in a subtropical coastal estuary on a spatiotemporal scale. Environ. Int. 154, 106558. https://doi.org/10.1016/j.envint.2021.106558.

Chen, M., Hur, J., 2015. Pre-treatments, characteristics, and biogeochemical dynamics of dissolved organic matter in sediments: a review. Water Res. 1 (79), 10–25. https://doi.org/10.1016/j.watres.2015.04.018.

Chen, M., Jaffé, R., 2014. Photo- and bio-reactivity patterns of dissolved organic matter from biomass and soil leachates and surface waters in a subtropical wetland. Water Res. 15 (61), 181–190. https://doi.org/10.1016/j.watres.2014.03.075.

Clark, C.D., Aiona, P., Keller, J.K., De Bruyn, W.J., 2014. Optical characterization and distribution of chromophoric dissolved organic matter (CDOM) in soil porewater from a salt marsh ecosystem. Mar. Ecol. Prog. Ser. 516, 71–83. https://doi.org/10.3354/meps10833.

Clark, C.D., Bowen, J.C., de Bruyn, W.J., Keller, J.K., 2019. Optical characterization of chromophoric dissolved organic matter (CDOM) and Fe (II) concentrations in soil porewaters along a channel-bank transect in a salt marsh. Estuaries Coasts 42, 1297–1307. https://doi.org/10.1007/s12237-019-00558-6.

Clark, C.D., Litz, L.P., Grant, S.B., 2008. Salt marshes as a source of chromophoric dissolved organic matter (CDOM) to Southern California Coastal waters. Limnol. Oceanogr. 53 (5), 1923–1933. https://doi.org/10.4319/lo.2008.53.5.1923.

Cory, R.M., Harrold, K.H., Neilson, B.T., Kling, G.W., 2015. Controls on dissolved organic matter (DOM) degradation in a headwater stream: the influence of photochemical and hydrological conditions in determining light-limitation or substrate-limitation of photo-degradation. Biogeosciences 12, 6669–6685. https://doi.org/10.5194/bg-12-6669-2015.

Dall'Osto, M., Vaqué, D., Sotomayor-Garcia, A., Cabrera-Brufau, M., Estrada, M., Buchaca, T., Soler, M., Nunes, S., Zeppenfeld, S., van Pinxteren, M., Herrmann, H., Wex, H., Rinaldi, M., Paglione, M., Beddows, D.C.S., Harrison, R.M., Berdalet, E., 2022. Sea ice microbiota in the Antarctic peninsula modulates cloud-relevant sea spray aerosol production. Front. Mar. Sci. 9, 1–21. https://doi.org/10.3389/fmars.2022.827061.

Deng, Z., He, Q., Manning, A.J., Chassagne, C., 2023. A laboratory study on the behavior of estuarine sediment flocculation as function of salinity, EPS and living algae. Mar. Geol. 459, 107029. https://doi.org/10.1016/j.margeo.2023.107029.

Diggle, R.M., Tait, D.R., Maher, D.T., Huggins, X., Santos, I.R., 2019. The role of pore water exchange as a driver of CO_2 flux to the atmosphere in a temperate estuary (Squamish, Canada). Environ. Earth Sci. 78 (11), 336. https://doi.org/10.1007/s12665-019-8291-3.

Eagle, M.J., Kroeger, K.D., Pohlman, J.W., Tamborski, J.J., Wang, Z.A., Brooks, T.W., Suttles, J.O., Mann, A., 2025. The $\delta^{13}C$ signature of dissolved organic and inorganic carbon reveals complex carbon transformations within a salt marsh. J. Geophys. Res. Biogeosci. 130. https://doi.org/10.1029/2025JG008898. e2025JG008898.

Ehleringer, J.D., Buchmann, N., Flanagan, L.B., 2000. Carbon isotope ratios in belowground carbon cycle processes. Ecol. Appl. 10, 412–422. https://doi.org/10.1890/1051-0761(2000)010[0412:CIRIBC]2.0.CO;2.

Fasching, C., Behounek, B., Singer, G.A., Battin, T.J., 2014. Microbial degradation of terrigenous dissolved organic matter and potential consequences for carbon cycling in brown-water streams. Sci. Rep. 4, 4981. https://doi.org/10.1038/srep04981.

Fellman, J.B., Hood, E., Spencer, R.G.M., 2010. Fluorescence spectroscopy opens new windows into dissolved organic matter dynamics in freshwater ecosystems: a review. Limnol. Oceanogr. 55 (6), 2452–2462. https://doi.org/10.4319/lo.2010.55.6.2452.

Gao, L., Gao, Y., Zong, H., Guo, L., 2019. Elucidating the hidden nonconservative behavior of DOM in large river-dominated estuarine and coastal environments of article. J. Geophys. Res., Oceans 124 (6), 4258–4271. https://doi.org/10.1029/2018JC014731.

Guimond, J., Tamborski, J., 2021. Salt marsh hydrogeology: a review. Water 13 (4), 1–23. https://doi.org/10.3390/w13040543, 543.

Guo, L., Santschi, P.H., Warnken, K.W., 1995. Dynamics of dissolved organic carbon (DOC) in oceanic environments. Limnol. Oceanogr. 40, 1392–1403. https://doi.org/10.4319/lo.1995.40.8.1392.

Guo, L., White, D.M., Xu, C., Santschi, P.H., 2009. Chemical and isotopic composition of colloidal organic matter from the Mississippi river plume. Mar. Chem. 114, 63–71. https://doi.org/10.1016/j.marchem.2009.04.003.

He, D., Li, P., He, C., Wang, Y., Shi, Q., 2022. Eutrophication and watershed characteristics shape changes in dissolved organic matter chemistry along two river-estuarine transects. Water Res. 214, 118196. https://doi.org/10.1016/j.watres.2022.118196.

Hedges, J.I., 1992. Global biogeochemical cycles: progress and problems. Mar. Chem. 39, 67–93. https://doi.org/10.1016/0304-4203(92)90096-S.

Herrmann, M., Najjar, R.G., Kemp, W.M., Alexander, R.B., Boyer, E.W., Cai, W.J., Griffith, P.C., Kroeger, K.D., McCallister, S.L., Smith, R.A., 2015. Net ecosystem production and organic carbon balance of U.S. east coast estuaries: a synthesis approach. Glob. Biogeochem. Cycles 29, 96–111. https://doi.org/10.1002/2013GB004736.

Huang, S.L., Chen, Y.N., Li, Y., 2020. Spatial dynamic patterns of salt marsh vegetation in southern Hangzhou Bay: exotic and native species. Water Sci. Eng. 13 (1), 34–44. https://doi.org/10.1016/j.wse.2020.03.003.

Huguet, A., Vacher, L., Relexans, S., Saubusse, S., Froidefond, J.M., Parlanti, E., 2009. Properties of fluorescent dissolved organic matter in the Gironde Estuary. Org. Geochem. 40, 706–719. https://doi.org/10.1016/j.orggeochem.2009.03.002.

Kaiser, K., Guggenberger, G., Zech, W., 1996. Sorption of DOM and DOM fractions to forest soils. Geoderma 74, 281–303. https://doi.org/10.1016/S00167061(96)00071-7.
Knobloch, A.L.J., Neale, P.J., Tzortziou, M., Canuel, E.A., 2022. Seasonal and tidal controls of the quantity and quality of dissolved organic matter at the marsh creek-estuarine interface. Estuar. Coast Shelf Sci. 278, 108124. https://doi.org/10.1016/j.ecss.2022.108124.
Knoke, M., Dittmar, T., Zielinski, O., Kida, M., Asp, N.E., de Rezende, C.E., Schnetger, B., Seidel, M., 2024. Outwelling of reduced porewater drives the biogeochemistry of dissolved organic matter and trace metals in a major mangrove-fringed estuary in Amazonia. Limnol. Oceanogr. 69 (2), 262–278. https://doi.org/10.1002/lno.12473.
Letourneau, M.L., Schaefer, S.C., Chen, H., McKenna, A.M., Alber, M., Medeiros, P.M., 2021. Spatio-temporal changes in dissolved organic matter composition along the salinity gradient of a marsh-influenced estuarine complex. Limnol. Oceanogr. 66 (8), 3040–3054. https://doi.org/10.1029/2018JG004982.
Li, H.-M., Tang, H.-J., Shi, X.Y., Zhang, C.-S., Wang, X.L., 2014. Increased nutrient loads from the Changjiang (Yangtze) River have led to increased harmful algal blooms. Harmful Algae 39, 92–101. https://doi.org/10.1016/j.hal.2014.07.002.
Li, K., Zhao, B., Han, L., Ge, T., Wang, N., Yao, P., 2024. Sediment porewaters serve as a transient organic carbon pool at the land-ocean interface. Water Res. 263, 122151. https://doi.org/10.1016/j.watres.2024.122151.
Li, M., Xie, W., Li, P., Yin, K., Zhang, C., 2020. Establishing a terrestrial proxy based on fluorescent dissolved organic matter from sediment pore waters in the East China Sea. Water Res. 182, 116005. https://doi.org/10.1016/j.watres.2020.116005.
Li, W., Zuo, S., Wang, H., Dong, J., Gao, T., Pan, S., Jin, B., 2019. Salt tide intrusion characteristics in main estuaries of China. Mar. Sci. Bull. 38 (6), 650–655. https://10.11840/j.issn.1001-6392.2019.06.006 (in Chinese with English abstract).
Lin, H., Bartlett, S.L., Guo, L., 2023. Distinct variations in fluorescent DOM components along a trophic gradient in the lower Fox River-Green Bay as characterized using one-sample PARAFAC approach. Sci. Total Environ. 902, 165891. https://doi.org/10.1016/j.scitotenv.2023.165891.
Lin, H., Guo, L., 2020. Variations in colloidal DOM composition with molecular weight within individual water samples as characterized by flow field-flow fractionation and EEM-PARAFAC analysis. Environ. Sci. Technol. 54 (3), 1657–1667. https://doi.org/10.1021/acs.est.9b07123.
Liu, J., Yu, X., Lin, X., Peng, T., Xue, L., Du, J., 2025. The importance of porewater exchange process on carbon lateral export from saltmarsh creek to coastal sea. J. Oceanol. Limno. 43, 90–102. https://doi.org/10.1007/s00343-024-3261-3.
Logozzo, L., Tzortziou, M., Neale, P., Megonigal, J.P., 2021. Photochemical and microbial degradation of colored dissolved organic matter exported from tidal marshes. J. Geophys. Res. Biogeosci. 126. https://doi.org/10.1029/2020JG005744. e2020JG005744.
Lu, D., Yuzao, Q., Gu, H., Dai, X., Wang, H., Gao, Y., 2014. Causative species of harmful algal blooms in Chinese coastal waters. Algol. Stud. 145, 145–168. https://doi.org/10.1127/1864-1318/2014/0161.
Lu, Q., He, D., Pang, Y., Zhang, Y., He, C., Wang, Y., Zhang, H., Shi, Q., Sun, Y., 2020. Processing of dissolved organic matter from surface waters to sediment pore waters in a temperate coastal wetland. Sci. Total Environ. 742, 140491. https://doi.org/10.1016/j.scitotenv.2020.140491.
Malone, T.C., Newton, A., 2020. The globalization of cultural eutrophication in the coastal ocean: causes and consequences. Front. Mar. Sci. 7, 670. https://doi.org/10.3389/fmars.2020.00670.
Martineac, R.P., Vorobev, A.V., Moran, M.A., Medeiros, P.M., 2021. Assessing the contribution of seasonality, tides, and microbial processing to dissolved organic matter composition variability in a Southeastern US Estuary. Front. Mar. Sci. 8, 781580. https://doi.org/10.3389/fmars.2021.781580.
Medeiros, P.M., Seidel, M., Dittmar, T., Whitman, W.B., Moran, M.A., 2015. Drought-induced variability in dissolved organic matter composition in a marsh-dominated estuary. Geophys. Res. Lett. 42, 6446–6453. https://doi.org/10.1002/2015GL064653.
Menendez, A., Tzortziou, M., Neale, P., Megonigal, P., Powers, L., Schmitt-Kopplin, P., Gonsior, M., 2022. Strong dynamics in tidal marsh DOC export in response to natural cycles and episodic events from continuous monitoring. J. Geophys. Res. Biogeosci. 127 (7). https://doi.org/10.1029/2022JG006863. e2022JG006863.
Moran, M.A., Hodson, R.E., 1994. Support of bacterioplankton production by dissolved humic substances from three marine environments. Mar. Ecol. Prog. Ser. 110 (2/3), 241–247. http://www.jstor.org/stable/24847594.
Murphy, K.R., Stedmon, C.A., Graeber, D., Bro, R., 2013. Fluorescence spectroscopy and multi-way techniques. PARAFAC, Anal. Methods 5, 6557–6566. https://doi.org/10.1039/C3AY41160E.
Nebbioso, A., Piccolo, A., 2013. Molecular characterization of dissolved organic matter (DOM): a critical review. Anal. Bioanal. Chem. 405 (1), 109–124. https://doi.org/10.1007/s00216-012-6363-2.
Nellemann, C., Corcoran, E., Duarte, C.M., Valdrés, L., Young, C.D., Fonseca, L., Grimsditch, G., 2009. Blue Carbon: the Role of Healthy Oceans in Binding Carbon. UN Environment, GRID-Arendal. https://www.grida.no/publications/145.
Nelson, N.G., Muñoz-Carpena, R., Neale, P.J., Tzortziou, M., Megonigal, J.P., 2017. Temporal variability in the importance of hydrologic, biotic, and climatic descriptors of dissolved oxygen dynamics in a shallow tidal-marsh creek. Water Resour. Res. 53 (8), 7103–7120. https://doi.org/10.1002/2016WR020196.
Niloy, N.M., Habib, S.A., Islam, M.L., Haque, M.M., Shammi, M., Tareq, S.M., 2023. Distribution, characteristics and fate of fluorescent dissolved organic matter (FDOM) in the Bay of Bengal. Mar. Pollut. Bull. 195, 115467. https://doi.org/10.1016/j.marpolbul.2023.115467.
Odum, E.P., 2002. Tidal marshes as outwelling/pulsing systems. In: Weinstein, M.P., Kreeger, D.A. (Eds.), Concepts and Controversies in Tidal Marsh Ecology, pp. 3–7. https://doi.org/10.1007/0-306-47534-0_1. Dordrecht.
Osburn, C.L., Mikan, M.P., Etheridge, J.R., Burchell, M.R., Birgand, F., 2015. Seasonal variation in the quality of dissolved and particulate organic matter exchanged between a salt marsh and its adjacent estuary. J. Geophys. Res. Biogeosci. 120, 1430–1449. https://doi.org/10.1002/2014JG002897.
Osburn, K., Amaral, J., Metcalf, S.R., Nickens, D.M., Rogers, C.M., Sausen, C., Caputo, R., Miller, J., Li, H., Tennessen, J.M., Bochman, M.L., 2018. Primary souring: a novel bacteria-free method for sour beer production. Food Microbiol. 70, 76–84. https://doi.org/10.1016/j.fm.2017.09.007.
Otero, E., Culp, R., Noakes, J.E., Hodson, R.E., 2003. The distribution and δ13C of dissolved organic carbon and its humic fraction in estuaries of southeastern USA. Estuar. Coast Shelf Sci. 56, 1187–1194. https://doi.org/10.1016/S0272-7714(02)00330-X.
Pinsonneault, A.J., Neale, P.J., Tzortziou, M., Canuel, E.A., Pondell, C.R., Morrissette, H., Lefcheck, J.S., Megonigal, J.P., 2021. Dissolved organic carbon sorption dynamics in tidal marsh soils. Limnol. Oceanogr. 66, 214–225. https://doi.org/10.1002/lno.11598.
Pitta, E., Zeri, C., 2021. The impact of combining data sets of fluorescence excitation-emission matrices of dissolved organic matter from various aquatic sources on the information retrieved by PARAFAC modeling. Spectrochim. Acta 258, 119800. https://doi.org/10.1016/j.saa.2021.119800.
Santos, I.R., Burdige, D.J., Jennerjahn, T.C., Bouillon, S., Cabral, A., Serrano, O., Wernberg, T., Filbee-Dexter, K., Guimond, J.A., Tamborski, J.J., 2021. The renaissance of Odum's outwelling hypothesis in 'Blue Carbon' science. Estuar. Coast Shelf Sci. 255, 107361. https://doi.org/10.1016/j.ecss.2021.107361.
Schiebel, H.N., Gardner, G.B., Wang, X., Peri, F., Chen, R.F., 2018. Seasonal export of dissolved organic matter from a New England salt marsh. J. Coast Res. 34, 939–954. https://doi.org/10.2112/JCOASTRES-D-16-00196.1.
Schiebel, H.N., Peri, F., Chen, R.F., 2020. Dissolved organic matter export from surface sediments of a New England salt marsh. Wetlands 40 (4), 693–705. https://doi.org/10.1007/s13157-019-01213-3.
Schmidt, F., Koch, B.P., Goldhammer, T., Elvert, M., Witt, M., Lin, Y.S., Hinrichs, K.U., 2017. Unraveling signatures of biogeochemical processes and the depositional setting in the molecular composition of pore water DOM across different marine environments. Geochem. Cosmochim. Acta 207, 57–80. https://doi.org/10.1016/j.gca.2017.03.005.
Seidel, M., Beck, M., Riedel, T., Waska, H., Suryaputra, I.G.N.A., Schnetger, B., Niggemann, J., Simon, M., Dittmar, T., 2014. Biogeochemistry of dissolved organic matter in an anoxic intertidal creek bank. Geochem. Cosmochim. Acta 140, 418–434. https://doi.org/10.1016/j.gca.2014.05.038.
Sholkovitz, E.R., 1975. Flocculation of dissolved organic and inorganic matter during the mixing of river water and seawater. Geochem. Cosmochim. Acta 40 (7), 831–845. https://doi.org/10.1016/0016-7037(76)90035-1.
Shutova, Y., Baker, A., Bridgeman, J., Henderson, R.K., 2014. Spectroscopic characterisation of dissolved organic matter changes in drinking water treatment: from PARAFAC analysis to online monitoring wavelengths. Water Res. 54, 159–169. https://doi.org/10.1016/j.watres.2014.01.053.
Skoog, A., Benner, R., 1997. Aldoses in various size fractions of marine organic matter: implications for carbon cycling. Limnol. Oceanogr. 42, 1803–1813. https://doi.org/10.4319/lo.1997.42.8.1803.
Stedmon, C.A., Nelson, N., 2015. The optical properties of DOM in the ocean. In: Hansell, D.A., Carlson, C.A. (Eds.), Biogeochemistry of Marine Dissolved Organic Matter, second ed. Elsevier, pp. 481–508. https://doi.org/10.1016/B978-0-12-405940-5.00010-8.
Stolpe, B., Guo, L., Shiller, A.M., Aiken, G.R., 2013. Abundance, size distributions and trace-element binding of organic and iron-rich nanocolloids in Alaskan rivers, as revealed by field-flow fractionation and ICP-MS. Geochem. Cosmochim. Acta 105, 221–239. https://doi.org/10.1016/j.gca.2012.11.018.
Stolpe, B., Zhou, Z., Guo, L., Shiller, A.M., 2014. Colloidal size distribution of humic- and protein-like fluorescent organic matter in the northern Gulf of Mexico. Mar. Chem. 164, 25–37. https://doi.org/10.1016/j.marchem.2014.05.007.
Tzortziou, M., Neale, P.J., Osburn, C.L., Megonigal, J.P., Maie, N., Jaffe, R., 2008. Tidal marshes as a source of optically and chemically distinctive colored dissolved organic matter in the Chesapeake Bay. Limnol. Oceanogr. 53, 148–159. https://doi.org/10.4319/lo.2008.53.1.0148.
Tzortziou, M., Zeri, C., Dimitriou, E., Ding, Y., Jaffé, R., Anagnostou, E., Pitta, E., Mentzafou, A., 2015. Colored dissolved organic matter dynamics and anthropogenic influences in a major transboundary river and its coastal wetland. Limnol. Oceanogr. 60 (4), 1222–1240. https://doi.org/10.1002/lno.10092.
Wang, A., Zhang, K., He, D., Fan, D., Sun, Y., 2021. Spatial distribution and controlling factors of dissolved organic matter composition in the Yangtze Estuary in summer. Geochimica 50 (3), 317–328. https://doi.org/10.19700/j.0379-1726.2021.03.009 (in Chinese with English abstract).
Weigelhofer, G., Jirón, T.S., Yeh, T.-C., Steniczka, G., Pucher, M., 2020. Dissolved organic matter quality and biofilm composition affect microbial organic matter uptake in stream flumes. Water 12, 3246. https://doi.org/10.3390/w12113246.
Weishaar, J.L., Aiken, G.R., Bergamaschi, B.A., Fram, M.S., Fujii, R., Mopper, K., 2003. Evaluation of specific ultraviolet absorbance as an indicator of the chemical composition and reactivity of dissolved organic carbon. Environ. Sci. Technol. 37, 4702–4708. https://doi.org/10.1021/es030360x.
Williams, C.J., Yamashita, Y., Wilson, H.F., Jaffé, R., Xenopoulos, M.A., 2010. Unraveling the role of land use and microbial activity in shaping dissolved organic matter characteristics in stream ecosystems. Limnol. Oceanogr. 55, 1159–1171. https://doi.org/10.4319/lo.2010.55.3.1159.
Wu, T., Wu, M., Xiao, J., 2008. Dynamics of community succession and species diversity of vegetations in beach wetlands of Hangzhou Bay. Chinese. J. Ecol. 27 (8), 1284–1289. https://doi.org/10.13292/j.1000 (in Chinese with English abstract).

Xiao, J., Wang, Z., Liu, D., Fu, M., Yuan, C., Yan, T., 2021. Harmful macroalgal blooms (HMBs) in China's coastal water: green and golden tides. Harmful Algae 107, 102061. https://doi.org/10.1016/j.hal.2021.102061.

Xiao, K., Zhang, L., Zhang, P., Wang, F., Wang, J., Chen, N., Li, Z., Pan, F., Lu, Z., Li, H., 2023. Tidal exchange of dissolved metal(loid)s and organic matters across the sediment-water interface in a salt marsh-mangrove ecotone. J. Hydrol. 622, 129665. https://doi.org/10.1016/j.marenvres.2025.107363.

Xie, D.F., Gao, S., Wang, Z.B., Pan, C.H., 2013. Numerical modeling of tidal currents, sediment transport and morphological evolution in Hangzhou Bay, China. Int. J. Sediment Res. 28, 316–328. https://doi.org/10.1016/S1001-6279(13)60042-6.

Xu, H., Houghton, E.M., Houghton, C.J., Guo, L., 2018. Variations in size and composition of colloidal organic matter in a negative freshwater estuary. Sci. Total Environ. 615, 931–941. https://doi.org/10.1016/j.scitotenv.2017.10.019.

Xu, H., Guo, L., 2017. Molecular size-dependent abundance and composition of dissolved organic matter in river, lake and sea waters. Water Res. 117, 115–126. http://digital.library.wisc.edu/1793/92660.

Xu, H., Guo, L., 2018. Intriguing changes in molecular size and composition of dissolved organic matter induced by microbial degradation and self-assembly. Water Res. 135, 187–194. https://doi.org/10.1016/j.watres.2018.02.016.

Yang, L., Cheng, Q., Zhuang, W.-E., Wang, H., Chen, W., 2019. Seasonal changes in the chemical composition and reactivity of dissolved organic matter at the land-ocean interface of a subtropical river. Environ. Sci. Pollut. Res. 26 (24), 24595–24608. https://doi.org/10.1007/s11356-019-05700-2.

Yuan, H.W., Chen, J.F., Ye, Y., Lou, Z.H., Jin, A.M., Chen, X.G., Jiang, Z.P., Lin, Y.S., Chen, C.T.A., Loh, P.S., 2017. Sources and distribution of sedimentary organic matter along the Andong salt marsh, Hangzhou Bay. J. Mar. Syst. 174, 78–88. https://doi.org/10.1016/j.jmarsys.2017.06.001.

Yunker, M.B., Belicka, L.L., Harvey, H.R., Macdonald, R.W., 2005. Tracing the inputs and fate of marine and terrigenous organic matter in Arctic Ocean sediments: a multivariate analysis of lipid biomarkers. Deep Sea Res. Part II Top. Stud. Oceanogr. 52, 3478–3508. https://doi.org/10.1016/j.dsr2.2005.09.008.

Zhang, X., Cao, F., Huang, Y., Tang, J., 2022. Variability of dissolved organic matter in two coastal wetlands along the Changjiang River Estuary: responses to tidal cycles, seasons, and degradation processes. Sci. Total Environ. 807 (3), 150993. https://doi.org/10.1016/j.scitotenv.2021.150993.

Zhang, Z., Yao, H., Wu, B., Wang, B., Chen, J., 2021. Limited capacity of suspended particulate matter in the Yangtze River Estuary and Hangzhou Bay to carry phosphorus into coastal seas. Estuar. Coast Shelf Sci. 258 (5), 107417. https://doi.org/10.1016/j.ecss.2021.107417.

Zhao, L., Gao, L., Thomas, D.N., 2024. Molecular size variations of chromophoric dissolved organic matter (CDOM) along a salinity gradient in the Changjiang River estuary. Estuar. Coast Shelf Sci. 297, 108606. https://doi.org/10.1016/j.ecss.2023.108606.

Zhou, Y., Li, Y., Yao, X., Ding, W., Zhang, Y., Jeppesen, E., Zhang, Y., Podgorski, D.C., Chen, C., Ding, Y., Wu, H., Spencer, R.G.M., 2019. Response of chromophoric dissolved organic matter dynamics to tidal oscillations and anthropogenic disturbances in a large subtropical estuary. Sci. Total Environ. 662, 769–778. https://doi.org/10.1016/j.scitotenv.2019.01.220.

Zhou, Y., Zhao, C., He, C., Li, P., Wang, Y., Pang, Y., Shi, Q., He, D., 2022. Characterization of dissolved organic matter processing between surface sediment pore water and overlying bottom water in the Yangtze River Estuary. Water Res. 215, 118260. https://doi.org/10.1016/j.watres.2022.118260.

Zhou, Z., Guo, L., Minor, E.C., 2016. Characterization of bulk and chromophoric dissolved organic matter in the Laurentian Great Lakes during summer 2013. J. Great Lake. Res. 42 (4), 789–801. https://doi.org/10.1016/j.jglr.2016.04.006.

Zhu, P., Chen, X., Zhang, Y., Zhang, Q., Wu, X., Zhao, H., Qi, L., Shao, X., Li, L., 2022. Porewater-derived blue carbon outwelling and greenhouse gas emissions in a subtropical multi-species salt marsh. Front. Mar. Sci. 9, 884951. https://doi.org/10.3389/fmars.2022.884951.